Research Article Vol. 36, No. 8 / August 2019 / Journal of the Optical Society of America B 1995

Journal of the Optical Society of America B

OPTICAL PHYSICS

Controlling fluorescence and noise correlation by phonon and double dressing in two types of Pr^{3+}:YSO

Abubakkar Khan,[1,†] Faizan Raza,[1,†] Irfan Ahmed,[2,3] Changbiao Li,[1] Al Imran,[1] Habib Ullah,[1] and Yanpeng Zhang[1,*]

[1]Key Laboratory for Physical Electronics and Devices of the Ministry of Education & Shaanxi Key Lab of Information Photonic Technique, Xi'an Jiaotong University, Xi'an 710049, China
[2]Department of Physics, City University of Hong Kong, Kowloon, Hong Kong SAR, China
[3]Electrical Engineering Department, Sukkur IBA University, Sukkur, 65200 Sindh, Pakistan
*Corresponding author: ypzhang@mail.xjtu.edu.cn

Received 23 January 2019; revised 29 May 2019; accepted 5 June 2019; posted 10 June 2019 (Doc. ID 358486); published 5 July 2019

We investigate the effect of single dressing and double dressing on fourth-order fluorescence (FL) and spontaneous four-wave mixing. The single dressing effect changes to a double dressing effect as we change the detuning (power) of the input beam from off-resonant (low power) to resonant point (high power). We also demonstrate the spectral and temporal nature of fourth-order FL and its Autler–Townes splitting caused by the competition of the phonon effect (at different temperatures) with a single and double dressed state in Pr^{3+}:Y_2SiO_5 crystal. To further explore the competition between the phonon and dressing effects, we investigated intensity-noise correlation of spontaneous parametric four-wave mixing at 110 K. Our results demonstrate the dependency of YSO crystal on temperature, detuning, and power, which can be controlled by the competition between a phonon with single and double dressing.

https://doi.org/10.1364/JOSAB.36.001995

1. INTRODUCTION

Improvement of light sources to enhance their stability and durability is the basic need of quantum optics. Lithium niobate was recently proposed for entanglement of high dimensions [1]. Compared to the other nonlinear doped crystals, Pr^{3+}:Y_2SiO_5 have distinctive properties. In Pr^{3+}:Y_2SiO_5 crystal, most research has been realized and conducted on enhanced four-wave mixing [2], light coherent storage [3–5], electromagnetically induced transparency (EIT) [6], and low- and higher-order FL [7]. Intensity-noise correlation is a good technique to realize entangled photon pairs [8]. Solid atom-like media such as rare-earth ion Pr^{3+} doped Y_2SiO_5(Pr^{3+}:YSO) is mostly used to demonstrate coherent effects owing to its long coherence time (0.1–1.0 s) and narrow spectral width (∼MHz) as compared to atomic gases [9–11]. Recently, the study of correlation is a good approach to know the response of Pr^{3+}:Y_2SiO_5 crystal. By using an external laser beam, correlated photon pairs have been achieved in Pr^{3+} :YSO crystal via spontaneous parametric four-wave mixing (SP-FWM) [12]. Wang *et al.* reported that by changing the polarization states of dressing fields and generating fields, the FL baselines, suppression, and Autler–Townes (AT) splitting of emission peaks can be controlled [13]. Lan *et al.* used the dressing effect to control the competition between the spontaneous parametric four-wave mixing and FL in a composite signal in Pr^{3+} :Y_2SiO_5 crystal [14]. Jiang *et al.* discussed that FL signal is a strong dressing due to the adiabatic population transfer between the dressed states [15].

The main objective of this paper is to control the fourth-order FL and intensity-noise correlation by interaction of a phonon with single and double dressing using temperature and laser parameters. Exploring competition between the dressing effect and phonon intensity by varying temperature and laser power is valuable for achieving quantum devices stability. Our results demonstrate that the phonon effect can significantly affect the nonlinear response of Pr^{3+} :Y_2SiO_5 crystal. The dressing phonon interaction plays a vital role in determining the controlling parameters of quantum optical devices such as temperature sensors and all-optical switching applications. Hence, we can control the dressing effect by the competition of a phonon with single and double dressing.

In this paper, we investigate the effects arising from the interaction of a phonon with a single and double dressed state of Pr^{3+}:Y_2SiO_5 crystal on output fourth-order FL and SP-FWM correlation. To demonstrate this, we chose variable power and detuning as intensive parameters of double dressing and the variable temperature of cryostat as an extensive parameter; with

such effects we are demonstrating AT-splitting of fourth-order FL in both the spectral and the time domain. We also presented the intensity-noise correlation between Stokes and anti-Stokes to further investigate the effects of laser power (low and high) with phonon interaction. In a V-type three level system, the lineshape of a measured correlation function changes from broad to sharp as the changing power of the input laser is changed from low to high, whereas the correlation is switched to anticorrelation as the power is reduced to low in a Λ-type three-level system.

2. EXPERIMENTAL SETUP AND BASIC THEORY

Our experiments are carried out in a rare-earth Pr^{3+}-doped Y_2SiO_5 crystal; the concentration of the Pr^{3+} ion is about 0.05% atom. Figure 1(a) shows the energy levels diagram of the Λ-type and V-type three-level system. Figure 1(b) shows the schematic diagram of the experimental setup. In our experiment, the sample was held in a cryostat (CFM-102) whose temperature was controlled by flowing liquid nitrogen. To investigate the effect of temperature and ensure the required temperature, liquid nitrogen flow was controlled precisely. We used two tunable dye lasers (a narrow scan with a 0.04 cm^{-1} linewidth) pumped by an injection-locked single-mode Nd:YAG laser (Continuum Powerlite DLS 9010,10 Hz repetition rate, 5 ns pulse width) to generate the fields $\boldsymbol{E}_1(\omega_1, \Delta_1)$ and $\boldsymbol{E}_2(\omega_2, \Delta_2)$ with the frequency detuning $\Delta_i = \omega_{mn} - \omega_i$ $(i = 1, 2)$; ω_{mn} is the corresponding atomic transition frequency between levels $|m\rangle$ and $|n\rangle$, and ω_i $(i = 1, 2)$ is the laser frequency. In the V-type system, the SP-FWM process is dressed by the $\boldsymbol{E}_1$ field (generating field) and the $\boldsymbol{E}_2$ field (dressing fields), which satisfy the phase-matching condition $\boldsymbol{k}_1 + \boldsymbol{k}_2 = \boldsymbol{k}_S + \boldsymbol{k}_{\mathrm{AS}}$, where $\boldsymbol{k}_{1,2}$ is the wavevector of the input fields and $\boldsymbol{k}_{S,\mathrm{AS}}$ is the wavevector of generated Stokes and anti-Stokes fields. Hence the SP-FWM process produces one Stokes and one anti-Stokes photon by absorption of two photons, accompanied by a FL signal. Similarly, Stokes and anti-Stokes outputs were obtained under a similar phase matching condition of SP-FWM in the Λ-type system. Arrangements of three photomultiplier tubes (PMT1-3) are used to detect the generated $\boldsymbol{E}_S, \boldsymbol{E}_{\mathrm{AS}}$, and FL composite signals [Fig. 1(b)]. One near

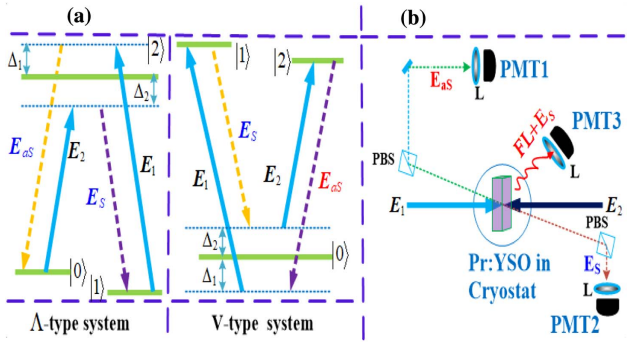

Fig. 1. (a) Three level Λ-type and V-type energy level. (b) Experimental setup, where PBS shows polarized beam splitter; PMT shows photomultiplier tube; and output Stokes, anti-Stokes and FL are marked as $\boldsymbol{E}_S$, $\boldsymbol{E}_{\mathrm{AS}}$, and FL, respectively.

and two far PMTs are placed at a distance of 11 cm and 118 cm from the cryostat, respectively. By scanning laser frequency, we obtained the spectral signals, and by fixing the laser frequency we obtained time domain signals. Stokes $\boldsymbol{E}_S$ and anti-Stokes $\boldsymbol{E}_{\mathrm{AS}}$ signals are reflected by polarized beam splitters (PBSs), which are detected at PMT2 and PMT1, respectively, whereas PMT3 detects the composite (FL + Stokes) signal.

A. Λ-Type System

In a Λ-type three-level system, by opening fields $\boldsymbol{E}_1$ and $\boldsymbol{E}_2$ the Stokes $\boldsymbol{E}_S$ and anti-Stokes $\boldsymbol{E}_{\mathrm{AS}}$ signals are generated with phase-matching condition $\boldsymbol{k}_S = \boldsymbol{k}_1 + \boldsymbol{k}_1' - \boldsymbol{k}_{\mathrm{AS}}$ and $\boldsymbol{k}_{\mathrm{AS}} = \boldsymbol{k}_1 + \boldsymbol{k}_1' - \boldsymbol{k}_S$, respectively. The perturbation chains for the $\boldsymbol{E}_S$ and $\boldsymbol{E}_{\mathrm{AS}}$ signals in the Λ-type system are written, respectively, as

$$\rho_{11}^{(0)} \xrightarrow{E_1} \rho_{21}^{(1)} \xrightarrow{E_{\mathrm{AS}}} \rho_{01}^{(2)} \xrightarrow{E_2} \rho_S^{(3)} (\rho_{21}^{(3)}),$$

$$\rho_{00}^{(0)} \xrightarrow{E_2} \rho_{20}^{(1)} \xrightarrow{E_S} \rho_{10}^{(2)} \xrightarrow{E_1} \rho_{aS}^{(3)} (\rho_{12}^{(3)}).$$

The third-order nonlinear density matrix elements of $\boldsymbol{E}_S$ and $\boldsymbol{E}_{\mathrm{AS}}$ with the self-dressing effect of $\boldsymbol{E}_1$ and the external-dressing field $\boldsymbol{E}_2$ can be written as

$$\rho_S^{(3)} = -iG_2 G_{\mathrm{AS}} \frac{(d_2\Gamma_{22} + |G_2|^2)}{(d_2(d_1 + |G_1|^2))} \frac{G_1}{(\Gamma_{01} + |G_2|^2/d_1)(d_3 + |G_1|^2/d_4 + |G_2|^2/\Gamma_{01})}, \tag{1}$$

$$\rho_{\mathrm{AS}}^{(3)} = \frac{-iG_2 G_S}{(d_2 + |G_1|^2/\Gamma_{10} + |G_2|^2/\Gamma_{00})} \frac{G_1}{(\Gamma_{10} + |G_1|^2/\Gamma_{11})(d_1 + d_0|G_1|^2/(d_0\Gamma_{22} + |G_2|^2))}, \tag{2}$$

where $d_0 = \Gamma_{20} + i\Delta_2$, $d_1 = \Gamma_{21} + i\Delta_1$, $d_2 = \Gamma_{20} + i\Delta_2$, $d_3 = \Gamma_{21} + i\Delta_2$, $d_4 = \Gamma_{11} - i\Delta'$, and $\Delta' = (\Delta_1 - \Delta_2)$. By opening both $\boldsymbol{E}_1$ and $\boldsymbol{E}_2$ simultaneously, the density matrix element of the fourth-order FL signal generated via perturbation chain $\rho_{11}^{(0)} \xrightarrow{E_1} \rho_{21}^{(1)} \xrightarrow{-E_1} \rho_{22}^{(2)} \xrightarrow{-E_2} \rho_{20}^{(3)} \xrightarrow{E_2} \rho_{22}^{(4)} \rho_{\mathrm{FL}}^{(4)}$ can be written as

$$\rho_{\mathrm{FL}}^{(4)} = \frac{|G_2|^2}{(d_1 + |G_1|^2/(d_4 + |G_2|^2/d_6))} \frac{|G_1|^2}{(\Gamma_{22} + |G_1|^2/\Gamma_{12} + |G_2|^2/d_5)(d_{20} + |G_1|^2/\Gamma_{10} + |G_2|^2/\Gamma_{00})}, \tag{3}$$

where $d_5 = \Gamma_{02} - i\Delta_2$ and $d_6 = \Gamma_{01} - i\Delta'$.

B. V-Type System

For the V-type system, the density matrix elements for the output $\boldsymbol{E}_S$ and $\boldsymbol{E}_{\mathrm{AS}}$ signal can be written via the dressed perturbation chains $\rho_{00}^{(0)} \xrightarrow{E_2} \rho_{02}^{(1)} \xrightarrow{E_{\mathrm{AS}}} \rho_{00}^{(2)} \xrightarrow{E_1} \rho_S^{(3)}$ and $\rho_{00}^{(0)} \xrightarrow{E_1} \rho_{10}^{(1)} \xrightarrow{E_S} \rho_{00}^{(2)} \xrightarrow{E_2} \rho_{\mathrm{AS}}^{(3)}$ as

$$\rho_S^{(3)} = \frac{-iG_1 G_{\mathrm{AS}}^*}{(d_0 + |G_2|^2/\Gamma_{00} + |G_1|^2/d_{21})(d_0 + d_0|G_1|^2/(d_0\Gamma_{00} + |G_2|^2))} \times \frac{G_2}{(d_{00} + |G_2|^2/(d_{10} + |G_2|^2/d_{20})) + |G_1|^2/(d'_{10} + |G_1|^2/d_{02})}, \tag{4}$$

$$\rho_{\mathrm{AS}}^{(3)} = \frac{-GG_1 G_{\mathrm{AS}}^*}{(d_{10} + d_0|G_1|^2/d_0\Gamma_{00} + |G_2|^2)(d_{20} + |G_2|^2/\Gamma_{22} + |G_1|^2/d_{11})} \times \frac{G_2}{(d'_{00} + |G_2|^2/[\Gamma_{20} + |G_2|^2/d_{21} + |G_1|^2/[\Gamma_{10} + |G_1|^2/d_{20}])}, \tag{5}$$

where

$$\begin{aligned} d'_{10} &= \Gamma_{10} - i\Delta', & d_{02} &= \Gamma_{02} - i\Delta_2, & d_{20} &= \Gamma_{01} - i\Delta_1, \\ d_{10} &= \Gamma_{20} - i\Delta', & d_{01} &= \Gamma_{10} + i\Delta_2 & d_{22} &= \Gamma_{22} + i\Delta', \\ d_{11} &= \Gamma_{21} - i\Delta', & d_{00} &= \Gamma_{00} - i\Delta', & d'_{00} &= \Gamma_{00} + i\Delta', \\ d_{21} &= \Gamma_{21} - i\Delta_1, \end{aligned}$$

Fourth-order FL, which can be generated via the pathway $\rho_{00}^{(0)} \xrightarrow{E_2} \rho_{20}^{(1)} \xrightarrow{-E_2} \rho_{00}^{(2)} \xrightarrow{E_1} \rho_{10}^{(3)} \xrightarrow{-E_1} \rho_{11}^{(4)}$, is given as

$$\rho_{\mathrm{FL}}^{(4)} = \frac{|G_2|^2}{(d_0 + |G_2|^2/\Gamma_{00})(\Gamma_{11} + |G_1|^2/d'_{11})} \times \frac{|G_1|^2}{(d_{01} + |G_1|^2/\Gamma_{00})(\Gamma_{00} + |G_1|^2/d_{01} + |G_2|^2/d'_{22})}, \tag{6}$$

where $d'_{11} = \Gamma_{12} + i\Delta'$ and $d'_{22} = \Gamma_{21} - i\Delta'$.

In the above equations $G_i = \mu_i E_i/\hbar$ is the Rabi frequency of field $\boldsymbol{E}_i$, with the electric dipole matrix elements μ_{ij} of levels $|i\rangle$ and $|j\rangle$, and Γ_{ij} is the transverse decay rate. Considering the interaction between the sample and coupling fields, the broadened linewidth of the measured FL signal can be described as $\Gamma_{ij} = \Gamma_{\mathrm{pop}} + \Gamma_{\text{ion-spin}} + \Gamma_{\text{ion-ion}} + \Gamma_{\mathrm{phonon}} - \Gamma_{\mathrm{dressing}}$, where $\Gamma_{\mathrm{pop}} = (2\pi T_1)^{-1}$ represents population decay time, which is associated with location of energy levels and the terms $\Gamma_{\text{ion-spin}} + \Gamma_{\text{ion-ion}} + \Gamma_{\mathrm{phonon}}$ are components of $(2\pi T_2^*)^{-1}$. Ion-spin coupling term $\Gamma_{\text{ion-spin}}$ is related to the effect of the individual ions, and $\Gamma_{\text{ion-ion}}$ is determined by the interactions among the ions of rare earth. Hence, this term can be controlled by the power of external field impurity concentrations. The phonon term Γ_{phonon} is associated with the sample temperature while the dressing term $\Gamma_{\mathrm{dressing}}$ is from dressing. In our experiment, the starting points of the pulse laser and measuring process are triggered simultaneously; the factor affecting the measured linewidth should include a coherence process between levels $|i\rangle$ and $|j\rangle$, which can be described as decoherence rate Γ_{10}, where $\Gamma_{ij} = (\Gamma_i + \Gamma_j)/2$.

The second-order correlation function $G_{ij}^{(2)}(\tau)$ between intensity fluctuations of two optical beams (i, j, $i \neq j$) as a function of time delay τ can be used to calculate the correlation between the generated outputs of SP-FWM, which is given as

$$G_{S-aS}^{(2)}(\tau) = \frac{\langle \delta I_S(t_S)\delta I_{aS}(t_{aS})\rangle |\theta(\tau)|^2}{\sqrt{\langle [\delta I_S(t_S)]^2\rangle \langle [\delta I_{aS}(t_{aS})]^2\rangle}} \cos(\Delta\varphi). \tag{7}$$

Here, $\Delta\varphi = \varphi_S - \varphi_{aS}$ represents the relative nonlinear phase between Stokes and anti-Stokes.

3. RESULTS AND DISCUSSION

Figures 2(a1)–2(a5) and 2(b1)–2(b5) show the spectral intensity of FL at different detuning Δ_2 (off-resonant and resonant) of $\boldsymbol{E}_2$ when Δ_1 is scanned from 604 to 607 nm in a V-type and Λ-type system, respectively. In a V-type system, one can predict the effects of the $\boldsymbol{E}_2$ and $\boldsymbol{E}_1$ dressing by looking at the FL density matrix defined in Eq. (6). From Eq. (6), the dressing terms $|G_1|^2/\Gamma_{12} + i\Delta_1 - i\Delta_2$ and $|G_2|^2/\Gamma_{21} + i\Delta_2 - i\Delta_1$ incorporate effects of both detuning (Δ_2 and Δ_1) and Γ_{phonon} related terms (Γ_{10}, Γ_{11}, Γ_{12}, Γ_{21}, Γ_{00} and Γ_{20}). In the V-type system, as we change the detuning Δ_2 while scanning Δ_1, the effect of the dressing terms from Eq. (6) is not very prominent, whereas the phonon effect is strong at 160 K. Phonon terms contribute more at high temperatures as Γ_{phonon} terms are related with the measured linewidth $\Gamma_{i/j}$, and the $\Gamma_{i/j}$ term increases with temperature as predicted by $\Gamma_{i/j} = \Gamma_{\mathrm{pop}} + \Gamma_{\text{ion-spin}} + \Gamma_{\text{ion-ion}} + \Gamma_{\mathrm{phonon}} - \Gamma_{\mathrm{dressing}}$. Therefore, by changing detuning Δ_2 of

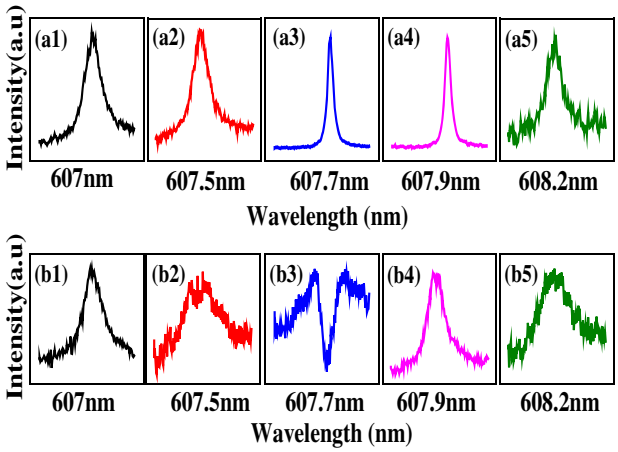

Fig. 2. (a1)–(a5) and (b1)–(b5) show spectral intensity of FL signal obtained at different detuning of $\boldsymbol{E}_2$ when $\boldsymbol{E}_1$ is scanned from 604 to 607 nm at fixed temperature of 160 K in V-type and Λ-type system energy levels, respectively.

$\boldsymbol{E}_2$ when the cryostat temperature is fixed at 160 k, the linewidth of the spectral signal shown in Figs. 2(a1)–2(a3) suggests that the resulting dressing effect can affect only the linewidth of the FL signal but cannot split the energy levels in the V-type system at 160 K. In the Λ-type system, by changing detuning Δ_2 of $\boldsymbol{E}_2$ at the crystal temperature of 160 k, the linewidth of the spectral signal changes along with the splitting as detuning approaches resonance ($\Delta_2 = 0$); that can be seen in Figs. 2(b1)–2(b3). Here, one can predict that AT-splitting is caused by the double dressing effect of $\boldsymbol{E}_2$ and $\boldsymbol{E}_1$ on the same energy level $|2\rangle$ suggested by the three dressing terms, $|G_2|^2/\Gamma_{01} + i(\Delta_1 - \Delta_2)$, $|G_1|^2/\Gamma_{11} + i(\Delta_1 - \Delta_2)$, and $|G_2|^2/\Gamma_{02} - i\Delta_2$ from Eq. (3). Interestingly, one can conclude that the contribution of the phonon effect on the lifetime of FL in the Λ-type system is less as compared to the V-type system. This difference is completely based on the dressing term derived in their respective density matrix from energy levels.

At resonance point ($\Delta_2 = 0$), strong AT-splitting is observed in the Λ-type system. Here, the phonon and dressing compete with each other as predicted by $\Gamma_{i/j} = \Gamma_{\text{pop}} + \Gamma_{\text{ion-spin}} + \Gamma_{\text{ion-ion}} + \Gamma_{\text{phonon}} - \Gamma_{\text{dressing}}$. Moreover, in the Λ-type system the strong dressing effect observed at resonant detuning [Fig. 2(b3)] does not change the lineshape of the FL signal as significantly as it effects the lineshape of the FL signal [Fig. 2(a3)] in the V-type system. As we change detuning from resonant to off-resonant, it can be observed that AT-splitting disappears again, and the linewidth of the FL curve increases due to the phonon broadening effect as shown in Figs. 2(b3)–2(b5).

Comparatively, at off-resonant detuning [Figs. 2(a1), 2(b1), 2(b1), and 2(b5)], the lineshape of the FL signal is broad, and the dressing effect is reduced due to the single dressing term ($|G_1|^2$), involving phonon terms Γ_{12}, Γ_{10}, Γ_{11} for the Λ-type system [mentioned in Eq. (3)] and Γ_{00}, Γ_{10} for the V-type system [mentioned in Eq. (6)]. While at $\Delta_2 = 0$ [Figs. 2(a3) and 2(b3)], the linewidth of the FL signal changes from broad to sharp involving phonon terms Γ_{00}, Γ_{10}, Γ_{12}, Γ_{21}, Γ_{11}, Γ_{02}, Γ_{01}, Γ_{20} for the Λ-type system and Γ_{00}, Γ_{10}, Γ_{11}, Γ_{20}, Γ_{12}, Γ_{21}, for the V-type system described by Eq. (3) and Eq. (6), respectively. The Λ-type system is more sensitive to dressing as compared to the V-type system, hence results in strong AT-splitting in the Λ-type system. The change in the signal linewidth and AT-splitting is attributed to competition between the phonon and dressing effect as predicted by $\Gamma_{i/j}$. The effect of the dressing and phonon competition on the measured lifetime Γ_{ij} is discussed in Fig. 4.

Figures 3(a1)–3(a5) and 3(b1)–3(b5) show the spectral intensity of FL by different detuning Δ_2 (off-resonant and resonant) of $\boldsymbol{E}_2$ when Δ_1 is scanned from 604 to 607 nm when the temperature is fixed at 120 K in a V-type and Λ-type three-level system, respectively. At off-resonant points [Figs. 3(a1), 3(a5), 3(b1), and 3(b5)], the FL signal shows low AT-splitting due to the single dressing effect $|G_1|^2$ competing with phonon terms (Γ_{12}, Γ_{11}, Γ_{10}) for the Λ-type system and (Γ_{00}, Γ_{10}) for the V-type system at a lower temperature than Fig. 2. At the resonant point [Figs. 3(a3) and 3(b3)], the signal shows strong AT-splitting involving phonon terms Γ_{00}, Γ_{10}, Γ_{12}, Γ_{21}, Γ_{11}, Γ_{02}, Γ_{01}, Γ_{20} in the Λ-type system and Γ_{00}, Γ_{10}, Γ_{11}, Γ_{20}, Γ_{12}, Γ_{21}, for the V-type system. The Λ-type system is more sensitive to double dressing $|G_1|^2$ and $|G_2|^2$, which results in stronger AT-splitting as compared to the V-type system. It should be noted that the contribution of the phonon effect in comparison to single and double dressing is less at 120 K as compared to 160 K. The phonon effect Γ_{phonon} decreases, and the double dressing effect is dominant, which result in obvious AT-splitting.

Figures 3(c1)–3(c5) and 3(d1)–3(d5) correspond to Figs. 3(a1)–3(a5) and 3(b1)–3(b5), respectively, but in the time domain. The sensitivity of the Λ-type system, with the dressing effect in comparison to the V-type system, can be observed by looking at the dip and delay of AT-splitting signals in the spectral and time domain, respectively, throughout the panels of Fig. 3. Comparing the results of Fig. 3 to the results

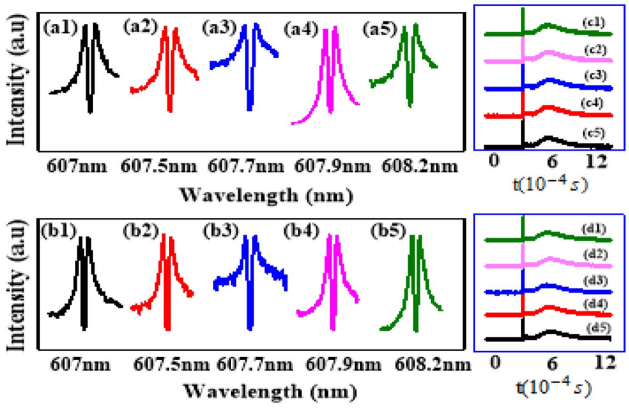

Fig. 3. (a1)–(a5) and (b1)–(b5) show spectral intensity of FL signal obtained at different detuning of $\boldsymbol{E}_2$ when $\boldsymbol{E}_1$ is scanned from 604 to 607nm at fixed temperature of 120 for V-type and Λ-type energy levels, respectively. (c1)–(c5) and (d1)–(d5) show corresponding temporal intensity of FL (a1)–(a5) and (b1)–(b5), respectively.

shown in Fig. 2, the effect of the phonon is less visible in Fig. 3 due to the low temperature (120 K) as compared to Fig. 2 (160 K). At the low temperature (120 K), the phonon term Γ_{phonon} is reduced, contributions from the phonon term in measured lifetime $\Gamma_{i/j}$ also decrease, and the reduced phonon term competes with dressing terms to determine the lifetime and lineshape of the FL signal.

In Fig. 4, we investigate the spectral and temporal intensity of the FL signal by changing the power of the incident beam and varying the temperature from high to low. Figures 4(a1)–4(a3) and 4(b1)–4(b3) show behavior of the FL signal when the power of $\boldsymbol{E}_1$ is decreased from high (7 mW) to low (1 mW) in both the V-type and Λ-type system, respectively.

As we decrease power of $\boldsymbol{E}_1$ from high to low, the intensity of the FL signal also changes accordingly. When the power of $\boldsymbol{E}_1$ is high [Figs. 4(a1) and 4(b1)], the dressing effect is strong due to contributions from both $|G_1|^2$ and $|G_2|^2$ terms. While at low power [Figs. 4(a3) and 4(b3)], the FL signal is dependent on only single dressing $|G_1|^2$. Therefore, one can say that by changing power from high to low, the dressing effect also becomes weak. Again AT-splitting in the Λ-type system [Fig. 4(b1)] is more obvious as compared to the V-type system [Fig. 4(a1)]. Figures 4(d1)–4(d3) and 4(e1)–4(e3) show the time domain intensity signal of FL corresponding to Figs. 4(a1)–4(a3) and 4(b1)–4(b3) for the V-type and the Λ-type system, respectively. One can see that AT-splitting is more obvious with the deeper dip in the Λ-type system as compared to the V-type system.

Figures 4(c1)–4(c4) and 4(f1)–4(f4) show the variation of AT-splitting at different temperatures. The phonon effect (Γ_{phonon}) is dominant at room temperature (300 K), so the linewidth of the FL intensity signal is broad. Moreover, the splitting distance of the dressed state level $\Delta_{\pm} = 2\sqrt{|G_1|^2 + |G_2|^2 - \Gamma_{\text{phonon}}}$ is low because of the phonon broadening effect. At 300 K, the phonon dominates the competition with dressing terms $|G_2|^2/\Gamma_{00}$, $|G_1|^2/d_1$, $|G_1|^2/\Gamma_{00}$, $|G_2|^2/d_2$ of the V-type system [Eq. (6)] and dressing terms $|G_1|^2/d_{11}$, $|G_2|^2/d_{12}$, $|G_1|^2/\Gamma_{12}$, $|G_2|^2/d_1$, $|G_1|^2/\Gamma_{10}$, $|G_2|^2/\Gamma_{00}$ of the Λ-type system [Eq. (3)], so weak AT-splitting is observed in Figs. 4(c1) and 4(f1). When the input field is scanned from 604 to 607 nm at fixed temperature of 77 K, the FL peak evolves from AT-splitting to a pure suppression dip. At 77 K, the dressing effect is strong whereas the phonon effect (Γ_{phonon}) is almost negligible. Because of the satisfaction of suppression condition $\Delta_1 + \Delta_2 = 0$ in the experiment, the suppression effect and AT-splitting depth are increased as shown in Figs. 4(c4) and 4(f4). Figures 4(f1)–4(f4) show the spectral intensity of the FL signal at a different temperature for V-type and Λ-type systems, respectively, since AT-splitting is increased from left.

The correlation function of the Stokes and anti-Stokes pair is calculated by time-dependent intensity fluctuations using Eq. (7). Figures 5(a1)–5(a3) and 5(b1)–5(b3) show the two-mode noise correlation between $\boldsymbol{E}_S$ and $\boldsymbol{E}_{\text{AS}}$ for the V-type system and the Λ-type system, respectively. As we change power from low to high, the lineshape of the calculated correlation changes to sharp from broad. This change in the lineshape can be described by the interaction of nested dressing terms and the phonon. At high power, the nested double dressing terms cancel each other, and the phonon terms (Γ_{phonon}) effects are more visible in the noise correlation. The competition occurs due to dressing terms ($|G_2|^2/\Gamma_{21} + i\Delta_1$, $|G_1|^2/\Gamma_{11} - i\Delta'$, $|G_2|^2/\Gamma_{01}$, $|G_1|^2/\Gamma_{10}$, $|G_2|^2/\Gamma_{00}$, $|G_1|^2/\Gamma_{11}$) incorporating phonon-related terms (Γ_{01}, Γ_{11}, Γ_{10}, Γ_{00}, Γ_{21}) as described by Eqs. (1) and (2) for the Λ-type system. Similar competition also occurs in the V-type system's dressing terms incorporating phonon-related terms (Γ_{22}, Γ_{01}, Γ_{00}, Γ_{21}) as described by Eqs. (4) and (5). The calculated noise correlation precisely follows the intensity of the Stokes/anti-Stokes lifetime given by the equation as

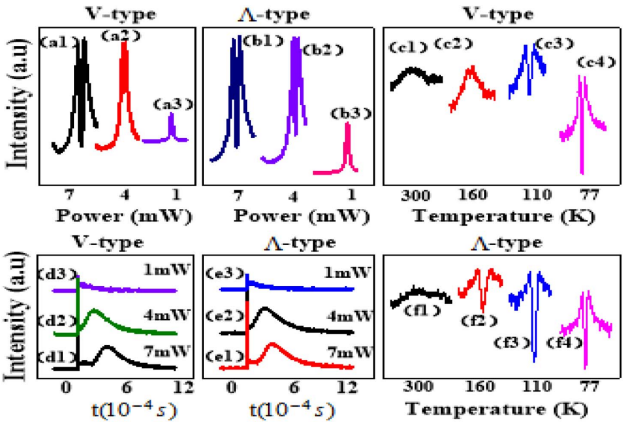

Fig. 4. (a1)–(a3) and (b1)–(b3) show the spectral intensity of fourth-order FL spectral detected at high (7 mW), medium (4 mW), and low (1 mW) power of $\boldsymbol{E}_1$ beam at fixed temperature of 120 K for V-type and Λ-type system, respectively. (c1)–(c4) and (f1)–(f4) show the spectral intensity of FL spectral detected at 300 K, 160 K, 110 K, and 77 K for V-type and Λ-type system, respectively. (d1)–(d3) and (e1)–(e3) correspond to (a1)–(a3) and (b1)–(b3), respectively, in time domain.

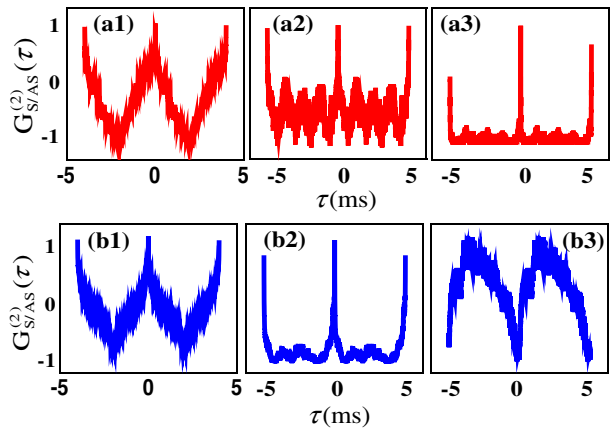

Fig. 5. (a1)–(a3) and (b1)–(b3) show two-mode intensity noise correlation of Stokes and anti-Stokes versus delayed time τ at medium temperature (110 K), by varying power from low to high of $\boldsymbol{E}_1$ for V-type and Λ-type energy levels, respectively.

$$A_{S/aS} = R_1|A_1|^2[\exp(-(2\Gamma^- + \zeta)|\tau|) + \exp(-(2\Gamma^- + \zeta)|\tau|) - 2\cos(\Omega_e|\tau|)\exp(-(\Gamma^+ + \Gamma^- + \zeta)|\tau|)],$$

where $\Gamma^{\pm} = \Gamma_{S/aS}$. As power increases, the lineshape of the correlation function changes from broad to sharp, and this trend is also obvious in all curves presented in Fig. 5. Besides the lineshape, the switching phenomenon is observed in the Λ-type system only at high power. Here, switching is related to nonlinear phase $\Delta\varphi = \varphi_S - \varphi_{AS} = 2(k_S n_2^S - k_{AS} n_2^{AS})|E_1|^2 e^{-r^2} z/n_1^{S/AS}$ between the Stokes and anti-Stokes signal modulated by the Kerr nonlinear gain at high power. The Kerr nonlinearity is characterized by a refractive index of $n_0 + n_2|E_1|^2$, where n_0 is the weak-field linear refractive index term, and $n_2 = 3\chi^{(3)}/2n_0$ is a nonlinear refractive index term proportional to the field strength $|E_1|^2$. Therefore, at high power, the relative nonlinear phase between Stokes and anti-Stokes is modulated to $\pi(\Delta\varphi = \pi)$ [16].

4. CONCLUSION

In summary, we presented the effects of single and double dressing with phonon competition in fourth-order FL in both the spectral and time domain by changing detuning and varying power under a different temperature state of YSO crystal in a multiatomic system. At off-resonant (low power), FL experienced single dressing and weak AT-splitting; however, by changing detuning to resonance (high power), FL experienced double dressing and strong AT-splitting. The dressing and phonon effect are found to be competing with each other. AT-splitting is gradually increasing as we decrease the temperature from high to low, which is attributed to the low phonon effect at a low temperature. We also performed the second-order correlation of Stokes and anti-Stokes and observed the effect of a phonon at low and high power. The change in the lineshape of the correlation was consistent in both the V-type and the Λ-type system. The phonon effect changes the nonlinear relative phase of correlated outputs by cross-phase modulation. However, the system demonstrated the switching of the correlation at the Λ-type system.

Funding. National Key R&D Program of China (2017YFA0303700, 2018YFA0307500); National Natural Science Foundation of China (NSFC) (11604256, 11804267, 61605154).

[†]These authors contributed equally to this work.

REFERENCES

1. H. Jin, P. Xu, X. W. Luo, H. Y. Leng, Y. X. Gong, W. J. Yu, M. L. Zhong, G. Zhao, and S. N. Zhu, "Compact engineering of path-entangled sources from a monolithic quadratic nonlinear photonic crystal," Phys. Rev. Lett. **111**, 023603 (2013).
2. B. S. Ham, M. S. Shahriar, and P. R. Hemmer, "Enhanced nondegenerate four-wave mixing owing to electromagnetically induced transparency in a spectral hole-burning crystal," Opt. Lett. **22**, 1138–1140 (1997).
3. A. V. Turukhin, V. S. Sudarshanam, M. S. Shahriar, J. A. Musser, B. S. Ham, and P. R. Hemmer, "Observation of ultraslow and stored light pulses in a solid," Phys. Rev. Lett. **88**, 23602 (2001).
4. J. J. Longdell, E. Fraval, M. J. Sellars, and N. B. Manson, "Stopped light with storage times greater than one second using electromagnetically induced transparency in a solid," Phys. Rev. Lett. **95**, 63601 (2005).
5. F. Beil, J. Klein, G. Nikoghosyan, and T. Halfmann, "Electromagnetically induced transparency and retrieval of light pulses in a Λ-type and a V-type level scheme in $Pr^{3+}:Y_2SiO_5$," J. Phys. B **41**, 74001 (2008).
6. B. S. Ham, M. S. Shahriar, M. K. Kim, and P. R. Hemmer, "Frequency-selective time-domain optical data storage by electromagnetically induced transparency in a rare-earth-doped solid," Opt. Lett. **22**, 1849–1851 (1997).
7. C. Li, L. Wang, H. Zheng, H. Lan, C. Lei, D. Zhang, M. Xiao, and Y. Zhang, "All-optically controlled fourth- and sixth-order fluorescence processes of Pr^{3+}:YSO," Appl. Phys. Lett. **104**, 51912 (2014).
8. Y. B. Sheng, L. Zhou, S. M. Zhao, and B. Y. Zheng, "Efficient single-photon-assisted entanglement concentration for partially entangled photon pairs," Phys. Rev. A **85**, 012307 (2012).
9. T. Zhong, J. M. Kindem, E. Miyazono, and A. Faraon, "Nanophotonic coherent light-matter interfaces based on rare-earth-doped crystals," Nat. Commun. **6**, 8206 (2015).
10. R. Z. Vered, Y. Shaked, Y. Ben-Or, M. Rosenbluh, and A. Pe'er, "Classical-to-quantum transition with broadband four-wave mixing," Phys. Rev. Lett. **114**, 063902 (2015).
11. Z. Qin, L. Cao, H. Wang, A. M. Marino, W. Zhang, and J. Jing, "Experimental generation of multiple quantum correlated beams from hot rubidium vapor," Phys. Rev. Lett. **113**, 023602 (2014).
12. V. Balić, D. A. Braje, P. Kolchin, G. Y. Yin, and S. E. Harris, "Generation of paired photons with controllable waveforms," Phys. Rev. Lett. **94**, 183601 (2005).
13. R. Wang, C. Lei, C. Li, H. Lan, H. Zheng, M. Xiao, and Y. Zhang, "Polarization dressed multi-order fluorescence of Pr3+:Y2SiO5," Phys. Chem. Chem. Phys. **16**, 15623–15629 (2014).
14. H. Lan, C. Li, C. Lei, H. Zheng, R. Wang, M. Xiao, and Y. Zhang, "Competition between spontaneous parametric four-wave mixing and fluorescence in Pr3+:YSO," Laser Phys. Lett. **12**, 015404 (2015).
15. T. Jiang, C. Li, I. Ali, R. Wang, Z. Li, and Y. Zhang, "Dressing role in fourth-order fluorescence and spontaneous parametric fourwave mixing," IEEE J. Quantum Electron. **52**, 9100106 (2016).
16. I. Ahmed, Z. Zhang, F. Wen, D. Zhang, C. Li, R. Wang, and Y. Zhang, "Switching correlation and noise level in Pr3+:YSO crystal via dressing nonlinear phase," Sci. Rep. **6**, 33568 (2016).